

GENERAL RELATIVISTIC SIMULATIONS OF EARLY JET FORMATION IN A RAPIDLY ROTATING BLACK HOLE MAGNETOSPHERE

SHINJI KOIDE

Faculty of Engineering, Toyama University, Gofuku 3190, Toyama 930-8555, Japan

DAVID L. MEIER

Jet Propulsion Laboratory, 4800 Oak Grove Drive, Pasadena, CA 91109

KAZUNARI SHIBATA

Kwasan and Hida Observatories, Kyoto University, Yamashina, Kyoto, 607-8471, Japan

AND

TAKAHIRO KUDOH

National Astronomical Observatory, Mitaka, Tokyo 181-8588, Japan

Received 1999 January 11; accepted 2000 January 21

ABSTRACT

To investigate the formation mechanism of relativistic jets in active galactic nuclei and microquasars, we have developed a new general relativistic magnetohydrodynamic code in Kerr geometry. Here we report on the first numerical simulations of jet formation in a rapidly rotating ($a = 0.95$) Kerr black hole magnetosphere. We study cases in which the Keplerian accretion disk is both corotating and counter-rotating with respect to the black hole rotation, and investigate the first ~ 50 light-crossing times. In the corotating disk case, our results are almost the same as those in Schwarzschild black hole cases: a gas pressure-driven jet is formed by a shock in the disk, and a weaker magnetically driven jet is also generated outside the gas pressure-driven jet. On the other hand, in the counter-rotating disk case, a new powerful magnetically driven jet is formed inside the gas pressure-driven jet. The newly found magnetically driven jet in the latter case is accelerated by a strong magnetic field created by frame dragging in the ergosphere. Through this process, the magnetic field extracts the energy of the black hole rotation.

Subject headings: accretion, accretion disks — black hole physics — galaxies: jets — magnetic fields — methods: numerical — MHD — relativity

1. INTRODUCTION

Radio jets ejected from radio-loud active galactic nuclei (AGNs) sometimes show proper motion with apparent velocity exceeding the speed of light c (Pearson et al. 1981; Hughes 1991). The widely accepted explanation for this phenomenon, called superluminal motion, is relativistic jet flow in a direction along the observer's line of sight with a Lorentz factor greater than 2 (Rees 1966). Such relativistic motion is thought to originate from a region very close to the putative supermassive black hole which is thought to power each AGN (Lynden-Bell 1969; Rees 1984). On the other hand, the great majority of AGNs are radio quiet and do not produce powerful relativistic radio jets (Rees 1984). These two classes of active objects (radio loud and radio quiet) are also found in the black hole candidates (BHCs) in our own Galaxy. Objects with superluminal jets, such as GRS 1915+105 and GRO J1655–40, belong to the radio loud class (Mirabel & Rodriguez 1994; Tingay et al. 1995). Other objects such as Cyg X-1 and GS 1124–68 are relatively radio quiet and produce little or no jet.

What causes the difference between the two classes? Recent observations of the BHCs in our Galaxy suggest that the Galactic superluminal sources contain very rapidly rotating black holes (normalized angular momentum, $a \equiv J/[GM_{\text{BH}}^2/c] = 0.9\text{--}0.95$, where G and M_{BH} are the gravitational constant and black hole mass, respectively), while the black holes in Cyg X-1 and GS 1124–68 are spinning much less rapidly ($a = 0.3\text{--}0.5$) (Cui, Zhang, & Chen 1998). A similar rapidly rotating black hole is also suggested in the AGN of the Seyfert 1 galaxy MCG-6-30-15 by the X-ray satellite *ASCA* (Iwasawa et al. 1996). According to nonrela-

tivistic studies of magnetically driven jets from accretion disks by (Shibata & Uchida 1986; Kudoh & Shibata 1995, 1997a), the terminal velocity of the formed jet is comparable to the rotational velocity of the disk at the foot of the jet. Further nonrelativistic simulations of jet formation confirm these results (Kudoh & Shibata 1997b; Ouyed, Pudritz, & Stone 1997; Romanova et al. 1997; Ustyugova et al. 1999), except for the extremely large magnetic field/high jet-power case (Meier et al. 1997; Meier 1999) in which very fast jets can be produced. The rotation velocity at the innermost stable orbit of the Schwarzschild black hole ($r = 3r_s$) is $0.5c$, where $r_s = 2GM_{\text{BH}}/c^2$ is the Schwarzschild radius. In addition, it appears that the poloidal magnetic field strength in disks around nonrotating black holes may be not extremely strong if the magnetic field energy density is comparable with that of the radiation (Begelman, Blandford, & Rees 1984; Rees 1984). Therefore, a jet produced by MHD acceleration from an accretion disk around a nonrotating black hole should be subrelativistic and very weak. In fact, numerical simulations of jet formation in a Schwarzschild metric show only subrelativistic jet flow (Koide, Shibata, & Kudoh 1999b), except for the case when the initial black hole corona is in hydrostatic equilibrium rather than free fall (Koide, Shibata, & Kudoh 1998).

Several mechanisms for relativistic jet formation from rotating black holes have been proposed (Blandford & Znajek 1977; Takahashi et al. 1990). However, up until now no one has performed a self-consistent numerical simulation of the dynamic process of jet formation in a rotating black hole magnetosphere. To this end, we have developed a Kerr general relativistic magnetohydrodynamic

(KGRMHD) code. In this paper we report briefly on what we believe are some of the first calculations of their kind—simulation of jet formation in a rotating black hole magnetosphere.

2. NUMERICAL METHOD

We use a $3 + 1$ formalism of the general relativistic conservation laws of particle number, momentum, and energy and Maxwell equations with infinite electric conductivity (Thorne, Price, & Macdonald 1986). The Kerr metric, which describes the spacetime around a rotating black hole, is used in the calculation. When we use Boyer-Lindquist coordinates, $x^0 = ct$, $x^1 = r$, $x^2 = \theta$, and $x^3 = \phi$, the Kerr metric $g_{\mu\nu}$ is written as follows:

$$ds^2 = g_{\mu\nu} dx^\mu dx^\nu = -h_0^2 (cdt)^2 + \sum_{i=1}^3 h_i^2 (dx^i)^2 - 2h_3 \Omega_3 c dt dx^3. \quad (1)$$

By modifying the lapse function in our Schwarzschild black hole code ($\alpha = (1 - r_s/r)^{1/2}$) to be $\alpha = (h_0^2 + \Omega_3^2)^{1/2}$, and adding some terms of Ω_3 to the time evolution equations, we were able to develop a KGRMHD code relatively easily. (See Appendix C in Koide et al. 1999b for more details on this procedure and the meaning of symbols used.)

We use the zero angular momentum observer (ZAMO) system for the 3-vector quantities, such as velocity \mathbf{v} , magnetic field \mathbf{B} , electric current density \mathbf{J} , and so on. For scalars, we use the frame comoving with the fluid flow. The simulation is performed in the region $0.75r_s \leq r \leq 20r_s$, $0 \leq \theta \leq \pi/2$ with 210×70 mesh points, assuming axisymmetry with respect to the z -axis and mirror symmetry with respect to the plane $z = 0$. The assumptions of the symmetry tend to suppress the turbulence in the disk caused by Balbus-Hawley instability. A free boundary condition is employed at $r = 0.75r_s$ and $r = 20r_s$. In the simulations, we use simplified tortoise coordinates, $x = \log(r/r_H - 1)$, where r_H is the radius of the black hole horizon. To avoid numerical oscillations, we use a simplified TVD method (Davis 1984; Koide, Nishikawa & Mutel 1996; Koide 1997; Koide et al. 1999b). We checked the KGRMHD code by computing Kepler motion around a rotating black hole and comparing with analytic results (Shapiro & Teukolsky 1983).

3. RESULTS

The simulations were performed for two cases in which the disk corotates and counter-rotates with respect to the black hole rotation. Figures 1a–1c illustrate the time evolution of the counter-rotating disk case and Figure 1d the final state of the corotating case. These figures show the rest mass density (*color*), velocity (*vectors*), and magnetic field (*solid lines*) in $0 \leq R \equiv r \sin \theta \leq 7r_s$, $0 \leq z \equiv r \cos \theta \leq 7r_s$. The black region at the origin shows the inside of the black hole horizon. The angular momentum parameter of the black hole is $a = 0.95$ and the radius is $r_H = 0.656r_s$. The initial state in the simulation consists of a hot corona and a cold accretion disk around the black hole (Fig. 1a). In the corona, plasma is assumed to be in nearly stationary infall, with the specific enthalpy $h/\rho c^2 = 1 + \Gamma p/[(\Gamma - 1)\rho c^2] = 1.3$, where ρ is the rest mass density, p is the pressure, and Γ is specific heat ratio and set $\Gamma = 5/3$. Far from the hole, it becomes the stationary transonic solution exactly. The accretion disk is located at $|\cot \theta| \leq 0.125$, $r \geq r_D = 3r_s$ and the initial velocity of the disk is assumed

to be the velocity of a circular orbit around the Kerr black hole. The corotating disk is stable, but the counter-rotating disk is unstable in the region $R \leq 4.4r_s$. Except for the disk rotation direction, we use the same initial conditions in both cases. The mass density of the disk is 100 times that of the corona at the inner edge of the disk. The mass density profile is given by that of a hydrostatic equilibrium corona with a scale height of $r_c \sim 3r_s$. The disk is in pressure balance with the corona, and the magnetic field lines are perpendicular to the accretion disk. We use the azimuthal component of the vector potential A_ϕ of the Wald solution to set the magnetic field, which provides a uniform magnetic field far from the Kerr black hole (Wald 1974). Here the magnetic field strength far from the black hole is $0.3(\rho_0 c^2)^{1/2}$, where ρ_0 is the initial corona density at $r = 3r_s$. However, we do not use the time component of the vector potential A_t from Wald solution; instead, we use the ideal MHD condition $\mathbf{E} + \mathbf{v} \times \mathbf{B} = 0$ to determine the electric field \mathbf{E} . Here the Alfvén velocity and plasma beta value at the disk ($r = 3.5r_s$) are $v_A = 0.03c$ and $\beta \sim 3.4$, respectively.

Figure 1b shows the state at $t = 30\tau_s$, where τ_s is defined as $\tau_s \equiv r_s/c$. By this time the inner edge of the disk has rotated 0.75 cycles, if we assume the edge is at $R = 3r_s$.¹ Actually, the edge falls toward the black hole and rotates faster at $R = 2r_s$. The rapid infall produces a shock at $R = 3.1r_s$, and the high pressure behind it begins to produce the jet. This is the same pressure-driven jet formation process seen previously in the Schwarzschild case (Koide et al. 1999b).

Figure 1c shows the final state of the counter-rotating disk case at $t = 47\tau_s$ when the inner edge of the disk rotated 1.2 cycles. The accretion disk continues to fall rapidly toward the black hole, with the disk plasma entering the ergosphere and then crossing the horizon, as shown by the crowded magnetic field lines near $r = 0.75r_s$. The magnetic field lines become radial due to dragging by the disk infall near the black hole. The jet is ejected almost along the magnetic field lines. Its maximum total and poloidal velocities are the same, $v = v_p = 0.44c$ at $R = 3.2r_s$, $z = 1.6r_s$. The mass density plot (color) shows that the jet consists of two layers. One is an inner, low-density, fast, magnetically driven jet and the other is an outer, high-density, slow, gas pressure-driven jet. The latter comes from the disk near the shock at $R = 3.1r_s$ and is, therefore, similar to the gas pressure-driven jet of Koide et al. (1998). The former is new and has never been seen in the Schwarzschild black hole case. It comes from the disk near the ergosphere and is accelerated as follows. As there is no stable orbit at $R \leq 4.4r_s$, the disk falls rapidly into the ergosphere. Inside the static limit, the velocity of frame dragging exceeds the speed of light ($c\Omega_3/\alpha > c$), causing the disk to rotate in the *same* direction of the black hole rotation (relative to the fixed Boyer-Lindquist frame), even though it was initially counter-rotating. The rapid, differential frame dragging enhances the azimuthal magnetic field, which then accelerates the flow upward and pinches it into a powerful collimated jet. The energetics of this phenomena are discussed in the last section.

¹ To calculate inner disk rotation cycles, in this paper we always will assume that the inner edge is located at $R = 3r_s$, regardless of how far inward the edge actually has accreted.

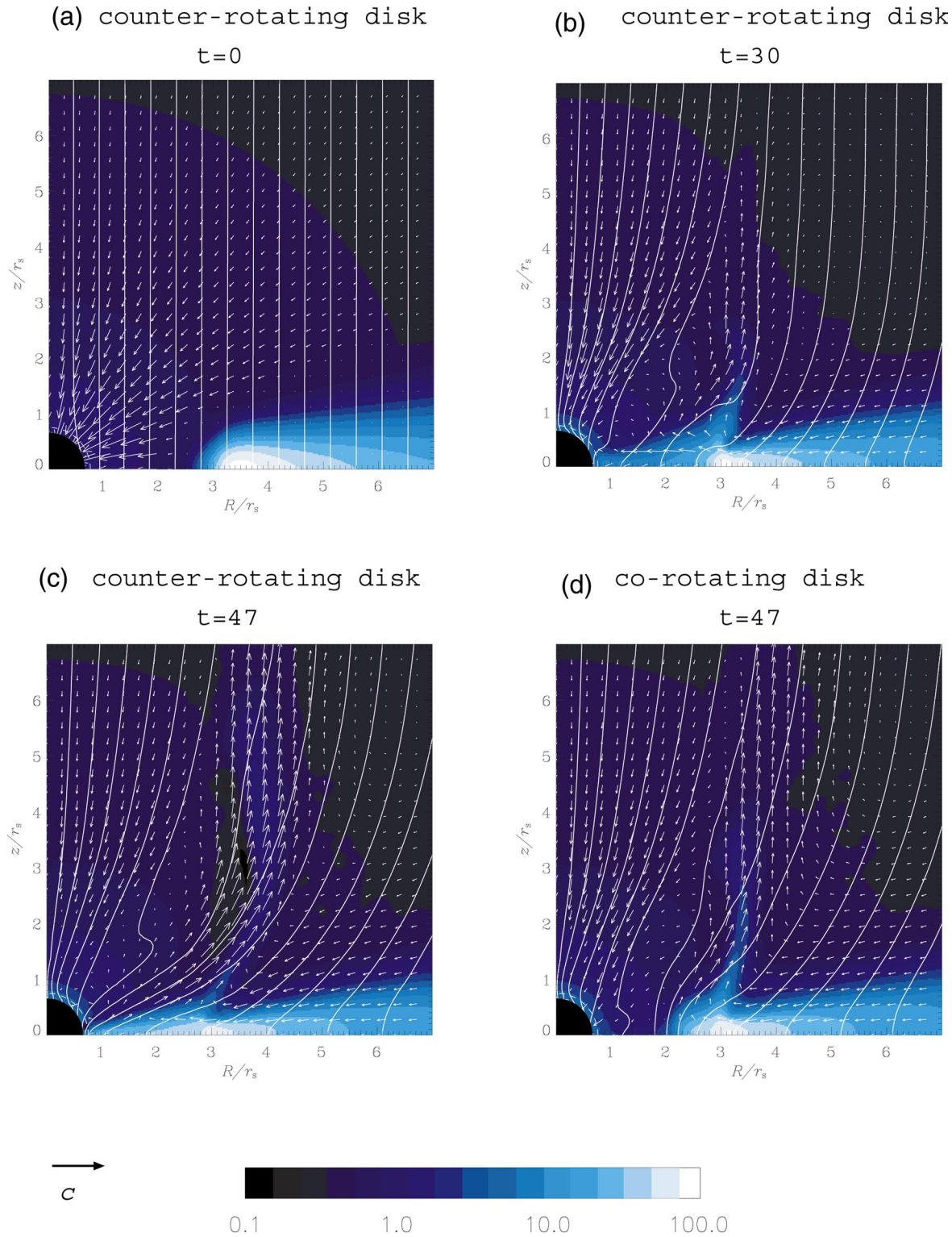


FIG. 1.—Time evolution of jet formation in the counter-rotating disk case and the final state of the corotating disk case. Color shows the logarithm of the proper mass density; vectors indicate velocity; solid lines show the poloidal magnetic field. The black fan-shaped region at the origin shows the horizon of the Kerr black hole ($a = 0.95$). The dashed line near the horizon is the inner boundary of the calculation region. At $t = 0$ and $t = 30\tau_s$ the state of the corotating and counter-rotating disk cases are almost identical. However, at $t = 47\tau_s$, while the infall of the disk in the corotating disk stops (due to a centrifugal barrier), the unstable orbits of the counter-rotating disk plasma continue to spiral rapidly toward the black hole horizon. This difference causes the magnetohydrodynamic jet formation mechanisms in the two cases to differ drastically, resulting in a powerful jet emanating from deep within the ergosphere.

Figure 1d shows a snapshot of the corotating disk case at $t = 47\tau_s$. The disk stops its infall near $R = 3r_s$ due to the centrifugal barrier with a shock at $r = 3.4r_s$. The high pressure behind the shock causes a gas pressure-driven jet with

total and poloidal velocities of $v = v_p = 0.30c$ at $R = 3.4r_s$, $z = 2.4r_s$. A detailed analysis shows that a weak magnetically driven jet is formed outside the gas pressure-driven jet with maximum total and poloidal velocities of $v = 0.42c$

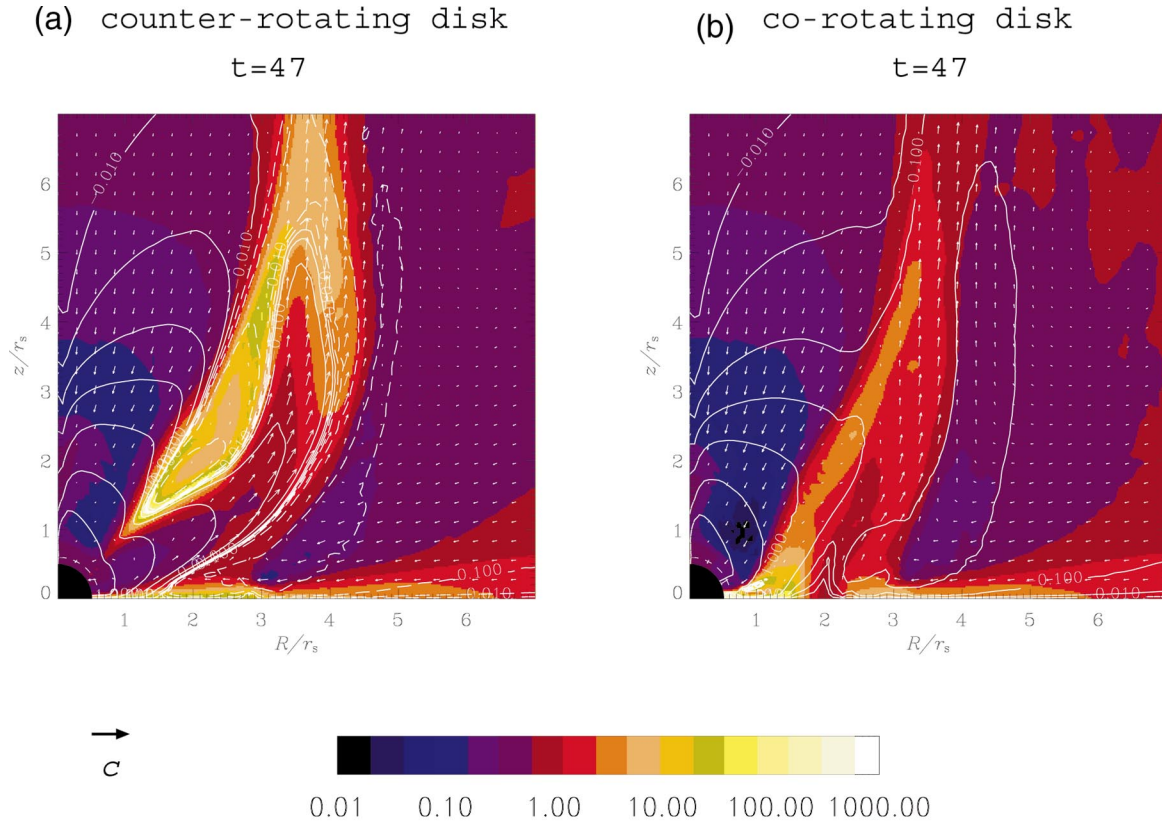


FIG. 2.—Plasma beta (color) and azimuthal component of the magnetic field B_ϕ (contour) in the counter-rotating and corotating disk cases. Solid lines show negative value of B_ϕ , and the dashed lines show positive values. The two cases differ significantly in structure, with the jet in the counter-rotating case originating much closer to the black hole.

and $v_p = 0.13c$, respectively. This two-layered shell structure is similar to that of Schwarzschild black hole case (Koide et al. 1998). The centrifugal barrier makes the disk take a much longer time to reach the ergosphere, which causes the difference between the corotating and counter-rotating disk cases.

To more fully illustrate the physics of the jet formation mechanism, in Figure 2 we show the plasma beta, $\beta \equiv p/(B^2/2)$ (color) and the toroidal component of the magnetic field, B_ϕ (contour) in the counter-rotating and corotating disk cases at $t = 47\tau_s$. The blue color shows the region where magnetic field dominates the gas pressure; light

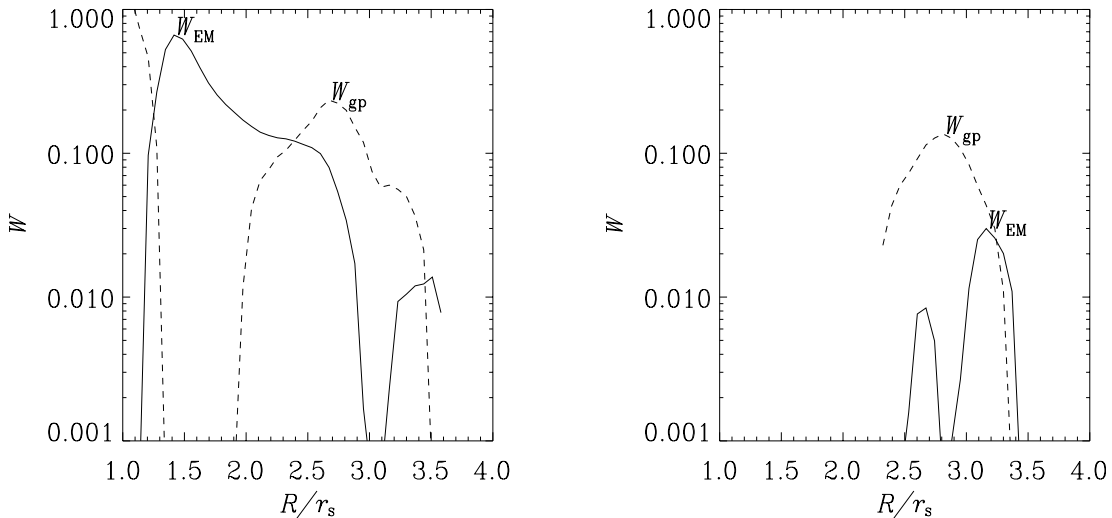


FIG. 3.—Power contribution to jet acceleration along the line, $z = 1.1r_s$ due to the gas pressure (W_{gp}) and the electromagnetic force (W_{EM}) for both the counter-rotating (a) and corotating (b) disk cases ($t = 47\tau_s$). The jet in the counter-rotating disk case is accelerated mainly by electromagnetic forces, while that in the corotating disk is accelerated mainly by gas pressure. Note that, while the power in the gas jet component is comparable in the two cases, the power in the MHD jet component is nearly 2 orders of magnitude greater in the counter-rotating case than the corotating case.

red—yellow shows where gas pressure is dominant; and the solid contour line shows the negative azimuthal magnetic field ($B_\phi < 0$), while the broken line shows the positive value ($B_\phi > 0$). The toroidal component of the magnetic field B_ϕ is negative and its absolute value is very large above the black hole in both cases. The field increases to more than 10 times the initial magnetic field. This amplification is caused by the shear of the plasma flow in the Boyer-Lindquist frame due to the frame-dragging effect of the rotating black hole (Yokosawa, Ishizuka, & Yabuki 1991; Yokosawa 1993; Meier 1999).

The distribution of the plasma beta (β) and the azimuthal component of the magnetic field (B_ϕ) of the counter-rotating and corotating disk cases are quite different. In the corotating disk case, they are similar to those of the Schwarzschild black hole case. In the counter-rotating disk case, the outer part has a positive azimuthal component of the magnetic field ($B_\phi > 0$), which is caused by the counter-rotating disk, and the outer part has the high plasma beta. The inner part has a negative azimuthal magnetic field ($B_\phi < 0$) and low plasma beta. Note that the very high plasma beta region (yellow region) is outside of the jet; at this point it has almost stopped and eventually will fall into the black hole. The negative azimuthal magnetic field is caused by the disk around the ergosphere, where the disk rotates in the same direction as the black hole in the Boyer-Lindquist frame.

To confirm the jet acceleration mechanism, we estimate the power from the electromagnetic field, $W_{EM} = v \cdot (E + J \times B)$ and the gas pressure, $W_{gp} = -v \cdot \nabla p$ along the line, $z = 1.1r_s$, which crosses the jet foot (Fig. 3). At $t = 47\tau_s$, the gas pressure is dominant in the corotating disk case (Fig. 3b). However, in the counter-rotating disk case, the electromagnetic power is dominant near the black hole even through the gas pressure power is the same as that of the corotating disk case (Fig. 3a). The magnetically driven jet in this latter case is accelerated by the magnetic field anchored to the ergospheric disk. The frame-dragging effect rapidly rotates the disk in the same direction as the black hole rotation, increasing the azimuthal component of the magnetic field and the magnetic tension which, in turn, accelerates the plasma by the magnetic pressure and centrifugal force, respectively. (A detailed analysis shows that both component of the magnetic forces are comparable.) This mechanism of jet production, therefore, is a kind of Penrose process that uses the magnetic field to extract rotational energy of the black hole and eject a collimated outflow from very near the horizon.

4. DISCUSSION

We have presented general relativistic simulations of jet formation from both counter-rotating and corotating disks in a Kerr black hole magnetosphere. We have found that jets are formed in both cases. At the time when the simulations were stopped ($t = 47\tau_s$ ($53\tau_s$), after the inner edge of the disk had rotated 1.2 (1.4) cycles in the counter-rotating (corotating) disk case) the poloidal velocities of the jets were $v \sim 0.4c$ (counter-rotating), $\sim 0.3c$ (corotating), both sub-relativistic. In the corotating disk case, the jet has a two-layered structure: inner, gas pressure-driven jet and outer, magnetically driven jet. On the other hand, in the counter-rotating case, a new magnetically driven jet has been found inside the gas pressure-driven jet. The new jet is accelerated by the magnetic field induced by the frame-dragging effect in the ergosphere. In this case, existence of a magnetically

driven jet is not clear outside the gas pressure-driven jet. A longer term simulation may show a three-layered structure including the outer, magnetically driven jet.

Here, we discuss briefly the energy transport from the magnetic field enhancement due to the frame-dragging effect of the rotating black hole to the newly found jet in the counter-rotating disk case. The detailed analysis of the transport (including spatial distribution and transport of energy and momentum) will be presented in our next paper. The general relativistic Maxwell equations yield the transport equation of the electromagnetic energy,

$$\frac{\partial e_\infty^{EM}}{\partial t} = -\nabla \cdot \mathbf{Q}^{EM} + \alpha W_{EM} + W_{fd},$$

where $e_\infty^{EM} \equiv \alpha[B^2/2 + E^2/(2c^2)] + \Omega_3(\mathbf{E} \times \mathbf{B})_\phi/c$ is the density of the collected electromagnetic energy, called *energy at infinity* of the electromagnetic field, \mathbf{Q}^{EM} is the electromagnetic energy flux density, and $W_{fd} \equiv -c\Omega_3[\rho_e E_\phi + (\mathbf{J} \times \mathbf{B})_\phi]$ with the electric charge density, ρ_e . The power density of the frame-dragging effect to the magnetic field energy increase is expressed by W_{fd} . The region where W_{fd} is significant is located almost exclusively in the ergosphere, and the value of W_{fd} is positive and huge ($W_{fd} \sim 3\rho_0 c^2/\tau_s$) in the region at $t = 47\tau_s$. The integration of W_{fd} over the region (L_{fd}) evaluates the magnetic field energy increase rate due to the frame-dragging effect. The numerical result of the counter-rotating disk case at $t = 47\tau_s$ provides $L_{fd} = 3.6\rho_0 c^3 r_s^2$. On the other hand, the integration of αW_{EM} over the jet-forming region (L_{EM}) evaluates the power of the electromagnetic field to the jet acceleration. The numerical result gives $L_{EM} = 0.72\rho_0 c^3 r_s^2$. This shows that about 20% of the frame-dragging power to the magnetic field is converted to the kinetic energy of the jet. The total kinetic energy of the jet is $K_{jet} = 0.77\rho_0 c^2 r_s^3$. Therefore, the electromagnetic field induced by the frame-dragging effect is capable of accelerating the jet plasma almost continuously.

It is important to understand where the energy of magnetic field amplification by frame dragging comes from—the rotating plasma or black hole itself. In the simple analysis below, we assume that the system is axisymmetric and neglect the motion of plasma in the poloidal direction. (Exact treatment will appear in our next paper.) Under these assumptions, the equation for the frame-dragging power density supplied to the magnetic field simplifies to $W_{fd} = -\partial(c\Omega_3 P_{gas}^\phi)/\partial t$. In this derivation, we have used the equation of motion for the gas, $\partial P_{gas}^\phi/\partial t = \rho_e E_\phi + (\mathbf{J} \times \mathbf{B})_\phi$, where P_{gas}^ϕ is the azimuthal component of the momentum density of the gas. The density of the corrected energy, called *energy at infinity* of the gas e_∞^{gas} , is expressed as $e_\infty^{gas} = \alpha[(e + p)\gamma - p] + c\Omega_3 P_{gas}^\phi$ (Thorne et al. 1986). The first term provides the rest mass energy density, kinetic energy density, thermal energy density, and *primitive* gravitational potential energy density. Here *primitive* means the potential depends only on the position. The second term, which we will refer to as $e_{fd} = c\Omega_3 P_{gas}^\phi$ here, appears only for Kerr black holes. That is, the potential depends not only on the position but also on the momentum of the gas. We can express the frame-dragging power density supplied to the electromagnetic field as $W_{fd} = -\partial e_{fd}/\partial t$. This shows that the energy source of the magnetic field amplification due to the frame-dragging effect comes from the energy release of the peculiar potential energy e_{fd} . When the potential energy density e_{fd} of a gas is released, the Lorentz force accelerates

the gas of the counter-rotating disk in an azimuthal direction opposite to the black hole rotation; that is, it imparts *negative angular momentum* to the counter-rotating gas. When the gas with the enlarged negative angular momentum falls into the black hole and is swallowed up by the hole, the angular momentum of the black hole decreases and the black hole rotational energy decreases (Meier 1999). Comparing the initial and final states, we can say that the rotational energy of the black hole is transported to the magnetic field energy. In other words, the black hole rotational energy is extracted by the magnetic field. In a similar scenario, the Penrose process extracts black hole rotational energy with the release of particle potential energy, corresponding to the peculiar potential energy density e_{fd} (Shapiro & Teukolsky 1983). To release the potential energy e_{fd} , the redistribution of the angular momentum of the matter is required because total angular momentum should be conserved (except at the black hole horizon). In the Penrose process, the redistribution of angular momentum is caused by the direct interaction between the particles, such as particle fission. In our case, the magnetic field plays a similar important role in the redistribution.

When the release of potential energy density e_{fd} is large enough and the density of the energy at infinity e_{∞}^{gas} is negative, the total energy of the black hole may decrease. This is the case in which the net energy of the rotational black hole is extracted. In our case, e_{∞}^{gas} is positive everywhere, and then the total energy of the black hole increases. In this case, the rotational energy of the black hole is converted into irreducible mass. Only the free energy of the rotating black hole is extracted to amplify the magnetic field and form the magnetically driven jet in the counter-rotating disk case.

The newly found magnetically driven jet is still sub-relativistic ($v_{\text{jet}} = 0.4c$) at $t = 47\tau_s$ in the counter-rotation case. Unfortunately, the counter-rotating (corotating) disk case could not be continued beyond $t = 47\tau_s$ ($t = 53\tau_s$) because of numerical problems. We have performed one other case previously—the infall of a magnetized non-rotating disk into a rapidly rotating black hole (Koide et al. 1999a). The disk falls toward the black hole more rapidly than the counter-rotating case. At later times (after almost two inner disk turns) it developed a *relativistic* jet with a velocity of $v \sim 0.9c$ (Lorentz factor ~ 2). We believe that, if we had been able to perform longer term simulations here, in at least the counter-rotating disk case the magnetically driven jet also would have been accelerated to relativistic velocities (and possibly the corotating case as well).

Our simulation results suggest that the relativistic jet is ejected in the counter-rotating disk case easier (at least, more quickly) than the corotating disk case. (However, this is not confirmed yet because of the limitation of the simula-

tion time.) The observed X-ray properties of the Galactic superluminal jet sources, GRO J1655–40 and GRS 1915+105, suggested that each contains a black hole spinning rapidly in the *same direction* as the accretion disk (Zhang, Cui, & Chen 1997). However, this does not mean that the relativistic jet is formed only with the corotating disk, that is, the plasma which radiates X-ray may be different from the source plasma which causes the relativistic jet. In fact, multiwavelength monitoring of the Galactic superluminal source GRS 1915+105 show that the onset of the jet ejection events are related to the sudden drop (with a number of sharp spikes) from a luminous state in the hard X-ray (Mirabel et al. 1996; Mirabel & Rodriguez 1998). This shows the disk becomes unstable when the jet is formed. For such a nonsteady disk, the method with the steady state disk assumption used by Zhang et al. (1997) may not be valid to determine the disk rotation direction. The unstable period may be caused by the counter-rotating plasma. Such reversal of the disk rotation is not so surprising, for example, the recent model of the transition between the hard and soft states of Galactic black hole candidate, Cyg X-1 with the reversal (Zhang, Cui, & Chen 1997). (Of course, the situation of microquasars and Cyg X-1 may be completely different. The Cyg X-1 disk reversal model is plausible because the companion star is a blue supergiant and the accretion onto the black hole appears to be fed by a stellar wind from that star. On the other hand, microquasars, GRS 1915+105 and GRO J1655–40, are low-mass binaries, thought to be accreting due to mass transfer through Roche lobe overflow. It is not clear whether a reversal can occur in such low-mass, Roche-lobe overflow binaries.) Furthermore, with respect to AGNs, the evidences for the counter-rotating disk or the rotation direction change have been discussed recently (see Lovelace & Chou 1996 and Kuznetsov et al. 1999 and references therein for further details regarding the observations). Detailed observations of the inner disk rotation in both Galactic superluminal sources and AGNs, especially during periods of jet ejection, will provide important clues to the jet formation mechanism in these objects.

S. K. thanks M. Inada-Koide for discussions and important comments for this study. We thank T. Nakamura, K.-I. Nishikawa, A. Tomimatsu, P. Hardee, and J.-I. Sakai for discussions and encouragement. We appreciate the support of the National Institute for Fusion Science and the National Astronomical Observatory in the use of their supercomputers. Part of this research was carried out at the Jet Propulsion Laboratory, California Institute of Technology, under contract with the National Aeronautics and Space Administrations.

REFERENCES

- Begelman, M. C., Blandford, R. D., & Rees, M. J. 1984, *Rev. Mod. Phys.*, 56, 255
 Blandford, R. D., & Znajek, R. 1977, *MNRAS*, 179, 433
 Cui, W., Zhang, S. N., & Chen, W. 1998, *ApJ*, 484, 383
 Davis, S. F. 1984, NASA Contractor Rep. 172373, ICASE Rep. 84-20
 Iwasawa, K., et al. 1996, *MNRAS*, 282, 1038
 Koide, S. 1997, *ApJ*, 478, 66
 Koide, S., Meier, D. L., Shibata, K., & Kudoh, T. 1999a, in *Proc. 19th Texas Symp. on Relativistic Astrophysics*, ed. E. Aubourg, T. Montmerle, & J. Paul (Singapore: World Scientific), in press
 Koide, S., Nishikawa, K.-I., & Mutel, R. L. 1996, *ApJ*, 463, L71
 Koide, S., Shibata, K., & Kudoh, T. 1998, *ApJ*, 495, L63
 ———. 1999b, *ApJ*, 522, 727
 Kudoh, T., & Shibata, K. 1995, *ApJ*, 452, L41
 ———. 1997a, *ApJ*, 474, 362
 ———. 1997b, *ApJ*, 476, 632
 Kuznetsov, O. A., Lovelace, R. V. E., Romanova, M. M., & Chechetkin, V. M. 1999, *ApJ*, 514, 691
 Lovelace, R. V. E., & Chou, T. 1996, *ApJ*, 486, L25
 Lynden-Bell, D. 1969, *Nature*, 223, 690
 Meier, D. L. 1999, *ApJ*, 522, 753
 Meier, D. L., Edgington, S., Godon, P., Payne, D. G., & Lind, K. R. 1997, *Nature*, 388, 350
 Mirabel, I. F., & Rodriguez, L. F. 1994, *Nature*, 371, 46
 ———. 1998, *Nature*, 392, 673
 Mirabel, I. F., Rodriguez, L. F., Chaty, S., Sauvage, M., Gerard, E., Duc, P.-A., Castro-Tirado, A., & Callanan, P. 1996, *ApJ*, 472, L111

- Ouyed, R., Pudritz, R. E., & Stone, J. M. 1997, *Nature*, 385, 409
Pearson, J. J., et al. 1981, *Nature*, 290, 365
Rees, M. J. 1966, *Nature*, 211, 468
———. 1984, *ARA&A*, 22, 471
Romanova, M. M., Ustyugova, G. V., Koldoba, A. V., Chechetkine, V. M., & Lovelace, R. V. E. 1997, *ApJ*, 482, 708
Shapiro, S. L., & Teukolsky, S. A. 1983, *Black Holes, White Dwarfs, and Neutron Stars* (New York: Wiley)
Shibata, K., & Uchida, Y. 1986, *PASJ*, 38, 631
Takahashi, M., Nitta, S., Tatematsu, Y., & Tomimatsu, A. 1990, *ApJ*, 363, 206
Thorne, K. S., Price, R. H., & Macdonald, D. A. 1986, *Membrane Paradigm* (New Haven: Yale Univ. Press)
Tingay, S. J., et al. 1995, *Nature*, 374, 141
Ustyugova, G. V., Koldoba, A. V., Romanova, M. M., Chechetkine, V. M., & Lovelace, R. V. E. 1999, *ApJ*, 516, 221
Wald, R. M. 1974, *Phys. Rev. D*, 10, 1680
Yokosawa, M. 1993, *PASJ*, 45, 207
Yokosawa, M., Ishizuka, T., & Yabuki, Y. 1991, *PASJ*, 43, 427
Zhang, S. N., Cui, W., & Chen, W. 1997, *ApJ*, 482, L155